Modeling the plastic relaxation onset in realistic SiGe islands on Si(001)

R. Gatti,[1,*] A. Marzegalli,[1] V. A. Zinovyev,[2] F. Montalenti,[1] and Leo Miglio[1]

[1]*Dipartimento di Scienza dei Materiali and L-NESS, Università degli Studi di Milano–Bicocca, Via Cozzi 53, I-20125 Milano, Italy*
[2]*Institute of Semiconductor Physics, Novosibirsk 630090, Russia*

A detailed investigation of plastic relaxation onset in heteroepitaxial SiGe islands on Si(001) is presented. The strain field induced by a straight misfit-dislocation segment is modeled by finite-element-method (FEM) calculations in three dimensions, fully taking into account the interaction with the multifaceted free surfaces of realistic islands. The total elastic energies before and after the placement of a 60° dislocation segment in the most favorable position are therefore evaluated by a full FEM approach, for different island sizes and compositions. The critical volumes with composition for inserting the dislocation are finally obtained and successfully compared with the data in a report by Marzegalli *et al.* [Phys. Rev. Lett. **99**, 235505 (2007)], where experimental values are compared to a simpler approach.

I. INTRODUCTION

Deposition of Ge on silicon substrates leads to Stranski-Krastanow growth.[1] After the formation of a thin wetting layer (WL), coherent three-dimensional (3D) islands[2,3] start forming, in order to release the elastic energy stored in the film, originated by the 4.2% Ge-Si lattice mismatch.[4,5] The nanometric size of such 3D structures immediately attracted considerable attention, in view of possible exploitation of optoelectronic devices. While islands based on III-V semiconductor compounds are better suited for realistic applications, Ge/Si systems are widely explored because they provide a simpler (purely covalent, fully miscible) system for the understanding of the complex physics involved in heteroepitaxial island formation and evolution. Recently, the closely related behavior of Ge/Si vs III-V compounds was nicely analyzed.[6,7]

In-depth experimental analysis of Ge/Si islands revealed a very fascinating physics, in particular for what concerns the morphological evolution during deposition of the 3D structures. It is known that islands grown by molecular-beam epitaxy (MBE) at common (500–800 °C) temperatures first appear as prepyramids and (105) pyramids (shallower in shape), and then as domes and barns (steeper morphologies, involving multiple exposed facets).[8–10] This evolution can be understood in simple thermodynamic terms. Islands with a large height-to-base aspect ratio (ρ) allow for a better volumetric strain relaxation[1,4,11] while involving a larger energy cost in terms of extra exposed surface (with respect to a flat WL). As a result, at small volumes islands are very shallow. Indeed, the observed pyramids are only 0.1 in ρ.[2,8] Following the changes in terms of aspect ratio, e.g., for islands grown at 700 °C,[10] a rapid increase occurs with volume, and coherent domes ($\rho \sim 0.2$) and barns ($\rho \sim 0.3$) are observed. Evolution toward higher aspect ratios, however, is abruptly interrupted by the opening of an alternative (plastic) channel for strain relaxation. Misfit dislocations are eventually injected, deeply influencing evolution at larger volumes. An intriguing cyclic-growth regime is actually observed, involving a periodic flattening of the island shape each time a new dislocation nucleates in the island,[12,13] generating an average decrease in ρ,

back to about 0.25–0.27 (superdome islands[14]). This drop in the aspect ratio is nicely highlighted also in Ref. 15, for samples grown by chemical-vapor deposition (CVD).

The issues influencing the critical size for plastic relaxation onset are the shape and the intermixing of the deposited Ge, with Si popping up from the substrate, which has been shown to decrease the Ge content with increasing growth temperatures, both in CVD (Ref. 15) and MBE growths.[16,17] Since alloying contributes to strain reduction, by lowering the effective lattice misfit, it competes with plastic relaxation,[18] effectively delaying the dislocation nucleation.[19] Interestingly, the same kind of effect (lowering of the effective misfit and delaying of the dislocation injection) was recently observed for growth on suitably pit-patterned substrates.[20]

In a recent letter,[19] we compared quite satisfactorily the experimental critical size for the onset of plastic relaxation in epitaxial SiGe islands on Si(001) of different compositions with our predictions based on a simple model. The latter was based on the partition of the total energy for an island with one dislocation segment into two contributions: the energy gain with respect to the lattice misfit, provided by the effective component of the Burgers vector for a 60° dislocation, and the energy cost originated by the additional lattice deformation due to the dislocation itself.[21] The first contribution was calculated using the Peach and Koehler force[22,23] describing the elastic interaction between the dislocation and the stress field of the coherent island, as calculated by finite-element method (FEM). The second contribution, i.e., the elastic self-energy of the dislocation segment, was analytically calculated as for a bulk SiGe lattice with no misfit strain. In particular, it was considered a cylindrical portion of the island as large as the geometric average of the distances between the nearest free surfaces and the dislocation position. This term is clearly approximated, but no sufficiently simple alternatives were available, at least for the complex shape provided by realistic SiGe islands.

In this paper we outline an improved strategy based on incorporating the stress field produced by a dislocation segment straightforwardly into the FEM simulation of the total elastic field in the SiGe islands with the free surfaces. By developing a suitable script for a commercial FEM package

(STRUCTURAL MECHANICS module of COMSOL MULTIPHYSICS), we are able to obtain in one time a virtually exact treatment of the fully converged elastic field of the dislocation-misfit segment and the one in the SiGe island with the free surfaces. We believe this strategy to be particularly valuable for any calculation of plastic relaxation, also in strained nanostructures, such as the ones obtained by state-of-the-art top-down lithography for microelectronic applications. The case of SiGe dislocated islands on Si(001) is however particularly interesting, as the presence of complex multifaceted free surfaces delimiting the nanosystem leads to a nontrivial modulation of the elastic field that cannot be predicted using simple analytical approach. In addition to that, due to the flat nature of the islands, the threading arms of the dislocation are understood to play a minor role with respect to a bulk system or a thick film, so that a model based purely on misfit segments is well suited.

The paper is organized as follows. In Sec. II we shall describe how we treated the plastic relaxation in the FEM framework, briefly overviewing alternative approaches. The reader more interested in results than in methodology can skip this section and go to Sec. III, which is devoted to an in-depth analysis of the strain and stress field within a realistic island, in the presence of a 60° misfit-dislocation segment. Here, results obtained with the FEM-based methodology in Sec. II are compared with large-scale atomistic calculations. In Sec. IV, the problem of calculating the critical volume for dislocation injection is tackled by using three different approaches: the original one in Sec. II, the Peach and Koehler method applied in Ref. 19, and a simpler analytical model usually applied to flat film, particularly useful in interpreting the differences between a thin film and a flat island. Finally, a direct comparison with the experimental data of Ref. 19 is presented in Sec. V, while Sec. VI summarizes our main results.

II. OUTLINE OF THE METHOD

Many different strategies have been developed for approaching defected structures. Atomistic simulations can be carried out in order to obtain atomic configurations around dislocation lines, core geometries, and energies (e.g., Refs. 24–28). A long computational time is however required so that, for instance, the simulation of dislocated island, despite the nanometer scale, can be performed only for idealized, prototypical cases (an example will be given in Sec. III).

An analytical approach is therefore highly desirable. The unavoidable consequent loss in the description of the core regions, when realistic structures are modeled, does not influence the calculation of mechanical properties because of their small extensions. Classical dislocation theory,[21] even if it remains the touchstone of all the tried analytical approaches, fails in managing complex three-dimensional structures with multiple surfaces and interfaces. Most of the models proposed in literature are developed considering dislocations described by analytical infinite-domain solutions and correction terms (image stresses) tackling surface and interface interactions, generally approximated by empirical or analytical formulas valid for simple boundary

geometries.[29] We propose a continuum-based approach exploiting the capability of numerical calculations to handle the interactions between dislocations and surfaces, as described in the following.

Let us consider first the general case of the calculation of the stress field due to a dislocation segment in a finite structure where no other sources of the elastic field are present. Classical elasticity theory describes the equilibrium state of a solid in terms of internal stresses $\sigma_{ij}(\mathbf{u})$, as a function of the displacement field $\mathbf{u}$ with respect to the initial position, and external applied forces f_i. Defining the body as the domain Ω, with boundary $\partial\Omega$, equilibrium equations can be written in a partial-differential-equation (PDE) problem as

$$\begin{cases} \sum_{j=1}^{3} \dfrac{\partial}{\partial x_j} \sigma_{ij}[\mathbf{u}(x,y,z)] = f_i & \text{if } (x,y,z) \in \Omega \\[2ex] \sum_{j=1}^{3} \sigma_{ij}[\mathbf{u}(x,y,z)]n_j = 0 & \text{if } (x,y,z) \in \partial\Omega_N, \quad i=1,2,3 \\[2ex] u_i(x,y,z) = 0 & \text{if } (x,y,z) \in \partial\Omega_D, \end{cases}$$
$$(1)$$

where $\partial\Omega_N$ are free-surface boundaries, $\partial\Omega_D$ are the fixed ones, and $\mathbf{n}$ is the vector normal to $\partial\Omega_N$. The finite-element method allows the numerical solving of equation system (1) so that by assigning the proper conditions it is possible to find the elastic field in any domain.

We conceived the use of the FEM calculation starting from the stress field of a dislocation segment in an infinite body and using the solver to find the solution that satisfies also the finite-body boundary conditions for free surfaces and interfaces. In particular, an external function is used in communicating to the FEM code the analytic stress tensor $\sigma_{ij}^{\text{dislo}}(\mathbf{u})$ ($i,j=1,2,3$) produced by a dislocation segment in a bulk.[21] Then, we replace in Eq. (1) $\sigma_{ij}(\mathbf{u})$ with $\sigma_{ij}(\mathbf{u}) + \sigma_{ij}^{0}(\mathbf{u})$, where $\sigma_{ij}^{0}(\mathbf{u}) = \sigma_{ij}^{\text{dislo}}(\mathbf{u})$ ($i,j=1,2,3$). The proper PDE problem is then solved also where no external forces are considered ($f_i=0$). When convergence is reached, the solution for $\sigma_{ij}(\mathbf{u})$ is found and the total stress tensor $\sigma_{ij}^{\text{tot}}(\mathbf{u})$ can be written as

$$\sigma_{ij}^{\text{tot}}(\mathbf{u}) = \sigma_{ij}^{\text{surf}}(\mathbf{u}) + \sigma_{ij}^{\text{int}}(\mathbf{u}) + \sigma_{ij}^{\text{dislo}}(\mathbf{u}), \qquad (2)$$

where $\sigma_{ij}^{\text{surf}}(\mathbf{u})$ is the correction to $\sigma_{ij}(\mathbf{u})$ due to the interaction between the dislocation and free surfaces [i.e., due to the first boundary condition in Eq. (1)], while $\sigma_{ij}^{\text{int}}(\mathbf{u})$ is the one due to the interaction between the extended defect and the interface (i.e., due to internal boundaries among different materials).[30]

The whole procedure has to be carried out taking into consideration that the bulk solution $\sigma_{ij}^{\text{dislo}}(\mathbf{u})$ ($i,j=1,2,3$) is singular along the dislocation line, so that some technical requirements for the FEM calculation are needed. A first obvious condition is that the mesh used to solve the PDE system must not contain nodes exactly along the dislocation line; otherwise, infinite values would be introduced. In addition, a sufficiently dense mesh must be defined close to the core region, where the stress field reaches high values, also in derivative. This second key requirement can be fulfilled

following a geometrical construction which also allows the quantitative estimates of the elastic energy in a dislocated structure. A small cylinder has been built around the dislocation line and we define a very dense array of nodes within it. We set the radius as $|\vec{b}|/\alpha$ with $\alpha=2.71$. Excluding only such small cylinder (about 1.5 Å in radius) in the elastic-energy calculation, the core contribution is empirically included (see, e.g., Refs. 21, 31, and 32). Notice that the definition of a suitable grid, as the one described above, is straightforward within several available FEM packages. Meshes, indeed, can be automatically generated by the codes, at variable levels of node density, based solely on the geometry of the objects composing the system. By introducing the very small cylinder explicitly, one automatically forces the mesh generator to introduce several nodes around the core region, as it was desired. However, a careful control of convergence as a function of the mesh density is mandatory. All the results presented in this paper were checked in terms of stability of the stress field and of the elastic energy, finding that data are converged when meshes containing more than 10^5 nodes are used. A detailed description of the dependence of the results on the mesh choice will be presented elsewhere.

To give a simple example of the flexibility and the accuracy of the method, we illustrate a case study where a direct comparison with the exact analytical solution is possible. Let us consider a dislocation with Burgers vector $\vec{b}$ and dislocation line $\vec{l}$ parallel to a single, horizontal free surface (placed at $x=0$). While for pure screw character the exact solution is provided by a simple image method,[21] it is more interesting to consider an edge dislocation. In this case, the problem is more complex, but it was nicely solved by Head,[33] who supplied a solution valid for any distance d between the dislocation line and the surface, in the case of Burgers vectors perpendicular to the free surface. The Head solution, in terms of various components of the stress tensor, is shown in the three upper panels of Fig. 1, while our results obtained by using FEM are displayed in the three lower ones. It is evident that a very good match is found. Outside the small cylinder around the dislocation line, indeed, the two solutions always differ by less than 0.1% of the stress value. Notice the stress-field behavior close to the surface: while the σ_{xx} and σ_{xy} stress components (parallel to the normal $\vec{n}$) vanish, σ_{yy} does not, at variance with the (wrong) result that one would obtain by using the approximated-image method.[21] It is therefore clear that our method is suitable for handling dislocations in the presence of free surfaces. Due to the requirement in terms of mesh density, a significant computer memory (up to 8 Gbyte for the results in Secs. III and IV) is needed to obtain stable results. Until a couple of years ago, this would have prevented similar calculations, so that smart attempts to circumvent the problem were proposed, avoiding dealing with the singularity directly in a FEM calculations. A particularly general and valid approach was introduced by Johnson and Freund[34] (JF), similar ideas being contained also in Ref. 27. JF proposed to suitably split the elastic problem into two subproblems. First, using the known analytical expression for $\sigma_{ij}^{\text{dislo}}$, tractions are computed at each free surfaces (components of the stress tensor normal to the surface itself). Then, a FEM calculation is performed for
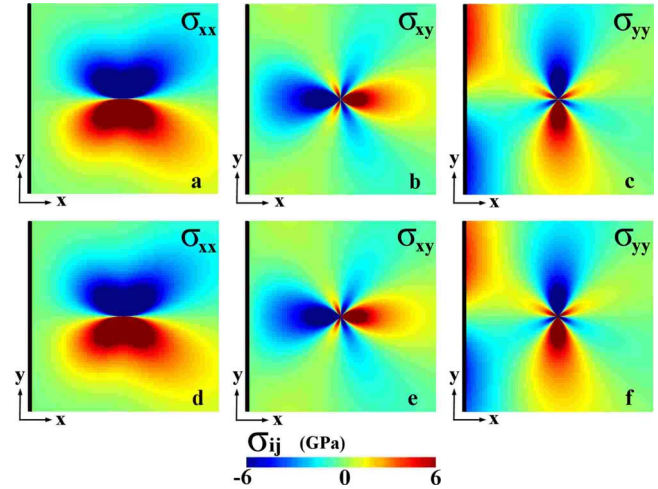
FIG. 1. (Color online) Panels (a)–(c): Various components of the edge dislocation stress field ($\vec{b}=[100]$, $\vec{l}=[001]$) near a (100) surface (black line), calculated using the analytical solution by Head (Ref. 33). The dislocation is placed at a distance of 6 nm from the surface. Panels (d)–(f): Corresponding results obtained by direct solution of the elastic problem by FEM.

the system without dislocation, but using such tractions (opposite in sign) as boundary conditions. The bulk stress field $\sigma_{ij}^{\text{dislo}}$ is finally superimposed. In this way, the problem of using very dense meshes while solving the elastic problem is bypassed.

Recently, another possible approach has been presented.[28,30,35] With respect to the JF method, no explicit analytical expressions for $\sigma_{ij}^{\text{dislo}}$ and no JF-type problem splitting are required. This *extended FEM* methodology seems very promising for treating systems containing several dislocations. However, some *ad hoc* technical FEM machinery needs to be implemented.

While the above methods are surely valid alternatives (we verified the perfect correspondence between our results and the JF approach for a simple test case) and might still prove to be essential for treating an elevated number of cores at the same time (a situation not encountered in this case[19]), our direct treatment of the dislocation field within FEM approach has some appealing features. First, it can be very easily implemented also within commercial FEM codes, where original sources are usually not available. A similar extension to use the method of Refs. 28, 30, and 35 does not seem straightforward. With respect to the JF method, on the other hand, one does not need to explicitly compute tractions. If their calculation poses no problems for simple geometries, for multifaceted heteroepitaxial islands one would need to carefully define the normal to each different exposed surface. In addition, if islands of different shapes need to be considered and compared, our direct approach allows one to move from one geometry to another very easily, particularly if the simple object-drawing features provided by most modern FEM packages are exploited.

In this section we have demonstrated that an accurate, direct solution of the elastic problem posed by a straight dislocation segment in the presence of free surfaces can be obtained directly by FEM. Let us now apply this methodology to realistic heteroepitaxial islands.
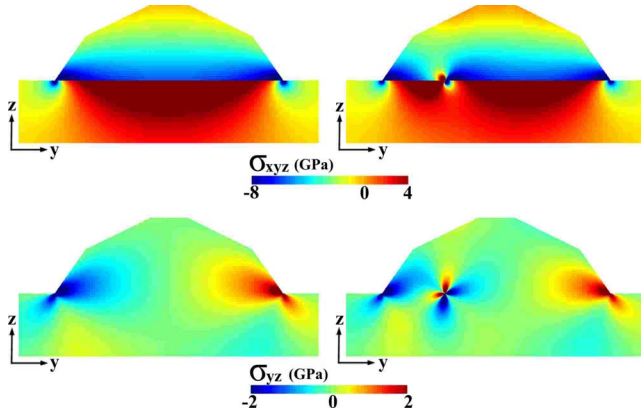
FIG. 2. (Color online) Hydrostatic (upper panels) and shear (bottom panels) stress components mapped in a central barn section. The left panels show the case of a coherent 35-nm-based island, while the right panels show the same system when a 60° dislocation is introduced.

III. MODELING OF THE DISLOCATED ISLAND

Before the onset of plastic relaxation, the elastic field in the island is completely determined by its shape and composition.[11] Indeed the lattice mismatch between Si and Ge [$(a_{Ge}-a_{Si})/a_{Si} \sim 4.2\%$, a_{Ge} and a_{Si} being the Ge and Si lattice parameters] generates a strained state of SiGe structures epitaxially grown on a Si substrate. In the 3D island configuration, free surfaces allow for a partial strain relaxation. Moreover a redistribution of the elastic energy between island and substrate occurs, giving rise to a strong modulation of the elastic field, depending on the actual facet number, extension, and inclination.[4,11] In this section we describe first how such field can be computed via FEM, with reference to the general PDE problem as written in Eq. (1).

The geometric details (actually the domain Ω) have to be fixed, for both the 3D island and the Si substrate (shapes, orientation, and dimensions). Then, the proper boundary condition over $\partial\Omega$ has to be imposed. We fixed the bottom of the substrate ($\mathbf{u}=0$), letting free the island surfaces. In Eq. (1) we replace $\sigma_{ij}(\mathbf{u})$ with $\sigma_{ij}(\mathbf{u})+\sigma_{ij}^0(\mathbf{u})$ $(i,j=1,2,3)$, where $\sigma_{ij}^0=\sigma_m\delta_{ij}$ in the island, reproducing the hydrostatic compression, as obtained directly from the lattice mismatch between the SiGe dot and the Si substrate (e.g., $\sigma_m \approx -8.6$ GPa for pure Ge), and $\sigma_{ij}^0=0$ in the substrate. A proper mesh is generated (it is particularly important to use a high number of nodes close to the island edges, where the solution is singular). The FEM solver calculates then the proper solution corresponding to the equilibrium state of the modeled system, obtaining the stress field in the elastically relaxed SiGe dot and in the substrate. In Fig. 2, left panels, we show the color maps for the hydrostatic stress and for a shear component of the stress tensor as obtained by FEM calculation when a pure Ge barn-shaped island[9,10] has been constructed. The hydrostatic stress maps reveal a strong compression taking place close to the island bottom edges while a base-to-top progressive relaxation is observed. The Si substrate below the island, on the other hand, experiences a tensile stress. This behavior was already observed in several papers, with the

quantitative details depending on the actual island shape. We can state that FEM is a suitable method for computing fast and accurately elastic properties in nanoscale system, as largely described in Ref. 11.

Let us move to the dislocated-island case. We shall recall that the calculation of the complex elastic field in a dislocated dot is the actual goal of our FEM methodology, and that the results here reported are a complete description of stress and strain field in realistically shaped 3D islands.

In Ref. 19 it was addressed that the onset of plastic relaxation in SiGe islands grown on a Si(001) substrate occurs in barn-shaped islands. We followed this suggestion and addressed the dislocated dots to be a barn. Moreover as in Ref. 19, we focused on perfect straight 60° dislocation segments (typical of Si and Ge diamond structure), the case of partial dislocations (30°–90° partials+stacking fault) often reported in literature (e.g., in Ref. 36) turning out to be more complex and will not be analyzed here. Different island compositions and sizes have been considered, along with different dislocation positions at the island-substrate interface (see Sec. V).

In Sec. II we described the procedure for calculating via FEM the elastic field in a finite system where the stresses are originated only by the presence of a dislocation segment. In one dislocated island, both the elastic field due to lattice misfit with the substrate and the one due to the dislocation are present instead. The superposition principle holding for linear system [as the one described in Eq. (1)] allows us to simply sum the two initial stresses $\sigma_{ij}^0(\mathbf{u})$ for one unique PDE problem. Therefore in Eq. (1) $\sigma_{ij}(\mathbf{u})$ becomes $\sigma_{ij}(\mathbf{u})+\sigma_{ij}^0(\mathbf{u})$ $(i,j=1,2,3)$, with

$$\begin{cases} \sigma_{ij}^0(\mathbf{u}) = \sigma_m\delta_{ij} + \sigma_{ij}^{\mathrm{dislo}}(\mathbf{u}) & \text{SiGe barn} \\ \sigma_{ij}^0(\mathbf{u}) = \sigma_{ij}^{\mathrm{dislo}}(\mathbf{u}) & \text{Si substrate.} \end{cases} \quad (3)$$

In particular, we choose to orient the dislocation line $\vec{l}$ along the [110] direction (here and in the following the direction of the x axis, the z axis being along [001] and y along [$\bar{1}$10]), and we take the Burgers vector $\vec{b}=(a_{Ge}/2)$[011]. Then the relative analytic stress tensor $\sigma_{ij}^{\mathrm{dislo}}(\mathbf{u})$ is obtained as in Ref. 21 for a dislocation segment actually starting on one side of the island and ending at the opposite one. We neglect the presence of threading arms and we place the dislocation segment always at the interface with the substrate. Both simplifications find their physical reason in a realistic picture of the dislocation evolution after its nucleation: the misfit segment has to be elongated as much as possible, in order to maximize the strain release, so that the threading arms have to become as short as possible and the dislocation has to move toward the interface.

Results for a pure Ge dislocated barn are plotted in right panels of Fig. 2, allowing for a close comparison with the coherent case (left panels). The island base was realistically set to 35 nm.[18,19] Notice the importance of specifying the islands' dimensions. The coherent case is self-similar, so that the stress field can be scaled to represent any island of the same shape. This is not possible anymore when a dislocation is considered since the Burgers vector introduces an intrinsic length scale. The dislocation was placed exactly at the inter-
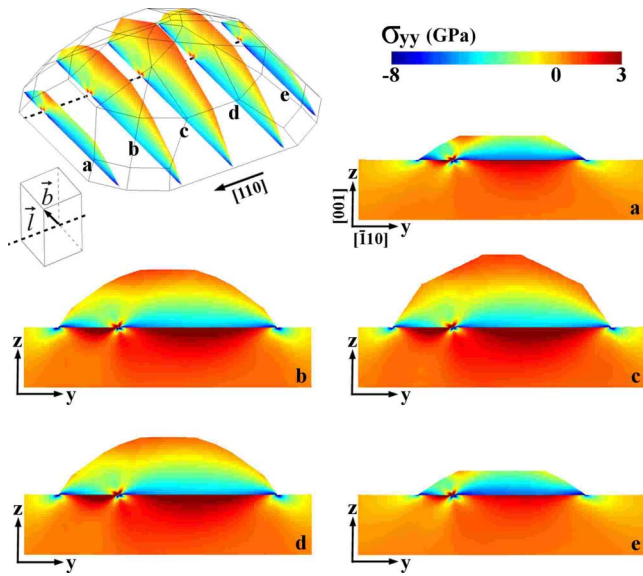
FIG. 3. (Color online) Elastic field in a 3D dislocated barn. Panels report color maps of the σ_{yy} component for different island cross sections, along the dislocation line. The cross sections in the island are shown in the top left panel, along with a sketch of dislocation line and Burgers vector orientation.

FIG. 4. (Color online) Left panel: Dome island as built in MD code. The facets are indicated and the {111} planes mostly involved in the initial deformation have been highlighted in color. Right panel: Sketch of the atomistic generation of the dislocation, z_0 being the interface level.

face at a relative distance of about 0.3 from the closest barn edge with respect to the island base, i.e., in the position that in Ref. 19 was indicated to be the lowest in total energy (as reported in Sec. IV we found exactly the same result).

Looking at the hydrostatic components σ_{xyz} (upper panels in the figure), it can be observed how the presence of the dislocation allows for a strong reduction in the compression at the island edge closer to the core, i.e., exactly where the elastic relaxation does not provide a good way for lowering the stress load arising from the lattice mismatch. The influence on the Si substrate is also interesting. Below the dislocation core, a compressive lobe is created. While this causes strong negative stress values right below the core, at larger distances it allows for a reduction in the tensile Si region. A detailed, quantitative analysis of the overall contribution to the total energy, allowing for an estimate of the critical volume for dislocation injection, will be presented in Secs. IV and V. The components σ_{yz} illustrated in the bottom panels of Fig. 2 give an example on the local modification induced by the 60° dislocation segment in reducing the shear deformation.

Proceeding with the analysis of the dislocation-induced stress field in the barn, in Fig. 3 we show the σ_{yy} component of the stress field at different positions within the island. We find the comparison between the various panels of Fig. 3 particularly appealing since it clarifies the complex interaction between the dislocation and the various island facets, highlighting the importance of performing actual three-dimensional calculations. The overall stress field is determined by several factors. Beside the position-dependent lattice-mismatch contribution, the relative position with respect to both the dislocation line and the free surfaces is important, together with the relative orientation of the Burgers vector (shown separately in the figure) and of the nor-

mal to the closer facet. In the cross section in Fig. 3(a), one observes a strong dislocation contribution reaching the free surface (upper left corner in the panel). In that region the dislocation core is very close to a free surface and, more importantly, the Burgers vector is almost normal to the facet. In cross section displayed in Fig. 3(e), the Burgers vector is instead parallel to the surface, causing a weaker relaxation close to the surface (orange area). Finally, in the central sections of the island [panels (b)–(d)], the typical butterfly-shaped dislocation stress field is observed to become less significant while moving from the base to the top, where the elastic relaxation is maximum.
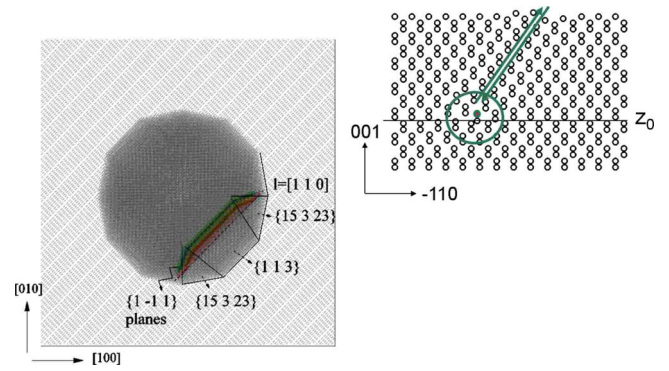
As a further confirmation of the method's accuracy, we chose to compare the elastic field of a dislocated island as found by our full FEM methodology with the same result calculated via atomistic simulations. We compare our results with molecular-dynamics (MD) ones based on the Tersoff empirical potential.[37,38] This comparison also allows for analyzing atomic-scale effects, which are not present in the continuum approach. Instead of a barn, we here consider a dome island[8] (see Fig. 4) since this allows us to reduce the number of atoms to be considered, still dealing with realistically sized and shaped islands. In order to introduce a 60° dislocation segment in the island analogous to the one previously treated by FEM, we applied the same procedure successfully used in Refs. 39 and 40 for the simpler case of a flat film. In particular, we chose to induce the dislocation in the shuffle set (in elastic-continuum calculations the dislocation setting is not relevant as no lattice is present). Briefly, a specific {111} glide plane is selected, together with the vertical position for the dislocation core. Suitably modulated rigid shears are applied above the core position: atoms on one side of the glide plane are sheared in the direction of the Burgers vector, while atoms at the other side are moved in the opposite one. In the left panel of Fig. 4 the island as built up in the MD code is shown from top view. The atomic planes mostly involved in the displacements are highlighted. The right panel of Fig. 4 contains a sketch of the procedure used to generate the dislocation.

After the preparation of the initial configuration, a simulated annealing procedure was run in order to minimize the
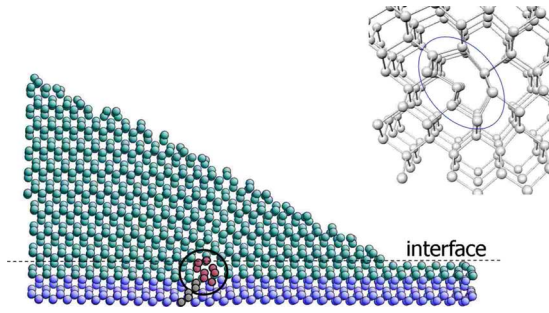
FIG. 5. (Color online) 60° dislocation in a dome island as obtained via atomistic simulation. The core position is encircled. Core atoms and the half extra plane are highlighted. The detailed atomistic configuration is shown in the right panel.

FIG. 6. (Color online) Color maps of the hydrostatic strain in the central cross section of a 3D dome island (32 nm in base) as obtained by FEM calculations (upper panel) and Tersoff-potential MD (bottom panel).

total energy in the dislocated configuration, reaching a temperature of 400 K before bringing the system down to zero temperature. The applied initial displacement is sufficient to guarantee that the minimization procedure causes only minor atomic arrangement around the induced dislocation core, disallowing the system to get back to the perfect-crystal configuration. During the simulation, periodic boundary conditions were applied in the directions parallel to the substrate, and the bottom four layers of the supercell were kept frozen to bulk position. The total system was composed of $\approx 1.5 \times 10^6$ atoms. 58 layers were used to describe the Si substrate, each of them composed of $\sim 21\,600$ atoms, completed by a 3 ML Ge wetting layer and by the dome island, made of about 118 000 Ge atoms.

Figure 5 presents a portion of the final configuration, highlighting the presence of a 60° shuffle dislocation segment at the island base. The core structure is shown in the right panel.

The same dome island[41] has been then constructed in the FEM code and a 60° dislocation has been introduced in the same position. In order to draw a closer comparison, we used the elastic constants predicted by the Tersoff potentials.[39,40] Panels in Fig. 6 show the color maps of the hydrostatic strain resulting from the two approaches. The good qualitative and quantitative correspondence is evident.

An obvious difference is seen close to the free surfaces, the steep dome facets being here stepped in their as-cut configuration. Each step is a source of alternating compressive and tensile regions, this effect being absent in the FEM calculation. Notice that the step-induced effect seen in the MD results is doubtfully realistic since reconstructions (unknown for the high-index facets of a dome) are expected to change the surface stresses. Moreover, the top (001) dome facet also is built up in the MD code without introducing possible reconstruction; random rebonding in dimers occurs during the simulated annealing, giving rise to local stresses.

Overall, the FEM approach, while recovering the correct result, allowed for a 2-orders-of-magnitude saving in computational time for this prototypical case. Estimating the critical volume for plastic relaxation (particularly at low Ge contents, yielding larger islands) by MD is prohibitive, so that in the following we shall drop the atomistic approach.
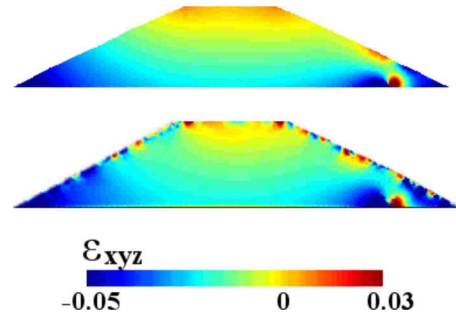
IV. ONSET OF PLASTIC RELAXATION IN EPITAXIAL SiGe ISLANDS

In Sec. III we have demonstrated that FEM calculations can yield a reliable description of the elastic field in a dislocated island. Before exploiting them to yield an accurate estimation of the critical volume for plastic relaxation onset, we find it interesting to introduce two more approximated (still analytic) approaches, in order to compare the different predictions and to understand which are the key contributions determining the system behavior.

On general grounds, the total elastic energy stored in a heteroepitaxial island in the presence of a dislocation can be written as

$$E_{\text{tot}} = E_{\text{coh}} + E_{\text{gain}} + E_{\text{cost}}, \qquad (4)$$

where E_{coh} is the elastic energy of the coherent dot; E_{gain} accounts for the energy lowering corresponding to the effective misfit reduction, provided by the dislocation; and E_{cost} is the energy of the additional lattice deformation produced by the defect. Different approaches can yield an explicit expression for the three terms contained in Eq. (4), at different levels of approximation.

A. Dislocation-position-independent model: Islands as effective thin films

A simple approach consists of using position-independent model (PIM) for the dislocation, commonly adopted in literature for the calculation of the critical thickness in films, and recently applied also for 3D GaAs islands.[42] Let us consider, first, the elastic energy stored in the island (E_{coh}) before the onset of plastic relaxation.

In a SiGe film grown on Si(001), the lattice mismatch causes a compression on the growth plane and an expansion in the vertical direction. In particular, denoting the misfit as $f = -(a_{\text{SiGe}} - a_{\text{Si}})/a_{\text{SiGe}}$ and referring to the axis as stated in Sec. III, a tetragonal strain described by $\varepsilon_{xx} = \varepsilon_{yy} = f$ and $\varepsilon_{zz} = -[\nu/(1-\nu)](\varepsilon_{xx} + \varepsilon_{yy})$ arises in the film. Relating to that case, the elastic strain energy in a 3D coherent island can be formulated as

TABLE I. Relaxation function $F_\nu(\rho)$ values for different island shapes and height-to-base aspect ratios, as calculated by FEM.

Shape	Aspect ratio	$F_\nu(\rho)$
105 pyramid	0.1	0.68
Dome	0.2	0.39
Barn	0.33	0.22

$$E_{\text{coh}} = \frac{G}{1 - \nu} F_\nu(\rho)(\varepsilon_{xx}^2 + 2\nu\varepsilon_{xx}\varepsilon_{yy} + \varepsilon_{yy}^2)V, \qquad (5)$$

where G is the shear modulus and ν is the Poisson ratio, V the island volume, while the factor $F_\nu(\rho)$ (named relaxation function, ρ being the aspect ratio) accounts for the energy reduction in the island, with respect to the film, due to the elastic relaxation. It is important to notice that Eq. (5) takes into account only the energy stored in the island, neglecting the contributions arising from the substrate elastic deformation (at variance with the other presented models as will be discussed in Sec. IV C). We numerically evaluated the relaxation function (using FEM) as $F_\nu(\rho) = W_{\text{coh}}/W_{\text{2D}}$. That is, we computed the ratio between the elastic-energy density (W_{coh}) in a coherent island, obtained as described in Sec. III, and the one in a biaxially strained two-dimensional (2D) layer constructed on the same substrate. The values of $F_\nu(\rho)$ for different island shapes are reported in Table I. While the relaxation function mainly depends on the aspect ratio, there is also a weak dependence on the detailed shape. Regardless of this issue, high aspect ratios provide better strain relaxation[11] and therefore lower values of $F_\nu(\rho)$.

Upon the formation of a misfit dislocation with dislocation line $\vec{l}$ oriented along the x axis, the strain component $\varepsilon_{xx} = f$ remains unchanged, whereas the perpendicular one is reduced to $\varepsilon_{yy} = f - \varepsilon_a$, where ε_a is that part of the misfit accommodated by the projection in the growth plane of the Burgers vector edge component (b_{eff}). By analogy with a 2D layer, ε_a can be simply calculated as $\varepsilon_a = b_{\text{eff}}\lambda/(\pi r^2)$, in the case of a circular-based island,[43] which is a suitable approximation for the barn basis. Here r is the island base radius and λ is the length of the dislocation line.

The PIM approach assumes that the energy contribution of dislocation can be estimated by a suitable average over different dislocation positions. For instance, the dislocation length is provided by the average extension of island along the x direction, $\lambda = (\pi/2)r$.[42] Thus, the energy associated with the misfit-relaxed 3D island containing one dislocation can be written as

$$E_{\text{incoh}} = \frac{G}{1 - \nu} F_\nu(\rho)[f^2 + 2\nu f(f - \varepsilon_a) + (f - \varepsilon_a)^2]V. \quad (6)$$

Therefore the energy gain due to the misfit-dislocation formation is

$$E_{\text{gain}} = E_{\text{incoh}} - E_{\text{coh}}. \qquad (7)$$

Let us now consider the expression for E_{cost}. In bulk systems, dislocation theory[21,42] provides the following expression for
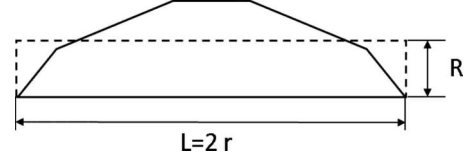
FIG. 7. Schematic representation of a barnlike island (solid line), which is approximated in the PIM calculation by a cylinder (dashed line) of equal base size $L = 2r$ and volume. The cylinder height is chosen as the cut-off radius R.

the energy stored in a cylinder of radius R around the dislocation line:

$$E_{\text{cost}} = \lambda \frac{G(1 - \nu \cos^2\beta)b^2}{4\pi(1 - \nu)} \ln\frac{\alpha R}{b}, \qquad (8)$$

where β is the angle between dislocation line and Burgers vector; α is the parameter which describes the energy of the dislocation core already introduced in Sec. II, set equal to 2.7 as in Ref. 42; and b is the length of the Burgers vector. For finite system, the role of the free surfaces in reducing the extension of the dislocation elastic field (see, e.g., Fig. 1) is commonly enclosed in the analytical model using a suitable choice of R as a cut-off radius of the dislocation self-field (e.g., in Ref. 42). We set, following the PIM view, R as the average distance between the interface and the free island facets. Considering again the barn as a 3D circular-based island of the same aspect ratio, R is given by

$$R = V/(\pi r^2). \qquad (9)$$

Figure 7 helps in understanding the geometric meaning of all the parameters.

B. Peach-Koehler approach

A more detailed procedure has to take into consideration the actual (position-dependent) interaction between the dislocation and the inhomogeneous elastic field of the island, before the onset of plastic relaxation. A combination of FEM calculations and dislocation theory provides a viable way.

The misfit reduction due to the presence of a dislocation can be viewed as the interaction between the strain field in the island and the dislocation Burgers vector: such an interaction depends, obviously, on the dislocation position. In details, the stress in the island, $\hat{\sigma}(x, y, z)$, exerts a force [Peach-Koehler (PK) force] $d\vec{F} = \vec{b} \cdot \hat{\sigma}(x, y, z) \times d\vec{l}$ on each infinitesimal segment of the dislocation line ($d\vec{l}$), $\vec{b}$ being the relative Burgers vector, moving the dislocation segment to the position maximizing strain relaxation in the island. The position-dependent energy gain term can be modeled as the work due to place a dislocation segment from outside the island into any position.[22,23]

Our results are referred to a 60° dislocation segment running along the x-axis direction ([110]) and with $\vec{b} = (a_{\text{SiGe}}/2)[011]$. The work performed by the Peach-Koehler force to place that segment from the outer of the island in any position (y_0, z_0) reads

$$E_{gain}(y_0, z_0) = \left[b_y \int_{z_0}^{h(y_0,z_0)} \left(\int_{l(y_0,z)} \sigma_{yy} dx \right) dz \right.$$
$$\left. + b_z \int_{z_0}^{h(y_0,z_0)} \left(\int_{l(y_0,z)} \sigma_{yz} dx \right) dz \right], \quad (10)$$

where $h(y_0, z_0)$ is the distance of the (y_0, z_0) position from the free surface along z, and $l(y_0, z)$ is the dislocation line length along x, which depends on z. Finally, b_y and b_z represent the components of the Burgers vector in the y ($[\bar{1}10]$) and in the z ($[001]$) directions, respectively. We recall that the integral of the Peach-Koehler force starting from the surface (energy $E=0$) is path independent if the stress field is calculated at the equilibrium, so that it is possible and convenient to calculate E_{gain} along a straight vertical path, from the surface to the most favorable position in the island (always along the interface with the substrate).

Let us consider now the E_{cost} term. We use the analytical formulation of Eq. (8), still taking R as a function of the dislocation position. In particular R is defined as the geometric average of the distances of the dislocation position from the base edge and the free surface above, as calculated in the middle cross section of the island. The limits of such approximation will be highlighted upon comparison with the full FEM results.

C. Comparison between different approaches

Figure 8 reports the three contributions E_{cost}, E_{gain}, and E_{tot}, as calculated in the case of a pure Ge barn (basis $L = 35$ nm) by the proposed full FEM methodology (Sec. II), by the PIM model, and by the PK approach. Actually, E_{tot} is shown in the third panel of Fig. 8 after subtraction of the corresponding coherent energy E_{coh}, so that positive (or negative) values indicate an overall energetic increase (or decrease) provided by the presence of the dislocation.

The calculation of the individual energy terms in the full FEM approach is done as follows. After the equilibrium condition is found, the FEM code provides the stress and strain fields, so that the total elastic energy in a volume V can be computed by the well-known relation

$$E = \frac{1}{2} \int_V (\sigma_{xx}\varepsilon_{xx} + \sigma_{yy}\varepsilon_{yy} + \sigma_{zz}\varepsilon_{zz} + 2\sigma_{xy}\varepsilon_{xy}$$
$$+ 2\sigma_{xz}\varepsilon_{xz} + 2\sigma_{yz}\varepsilon_{yz}) dV. \quad (11)$$

By integrating over the whole system volume, one would include in E the (wrong) contribution coming from the core region. We therefore integrate everywhere but for the small cylinder built around the core (see Sec. II). This yields the total elastic energy E_{tot}.[44] Following the definition, E_{cost} is actually given by the elastic energy in the zero-misfit island, when only the dislocation is present, so that E_{gain} can be directly computed by subtraction.

The comparison of the E_{cost} terms shown in the first panel of Fig. 8 clearly reveals some limitations of the PK treatment, where the influence of free surfaces on the dislocation field is described only by the introduction of a cut-off radius R related to the island geometry. An immediate consequence
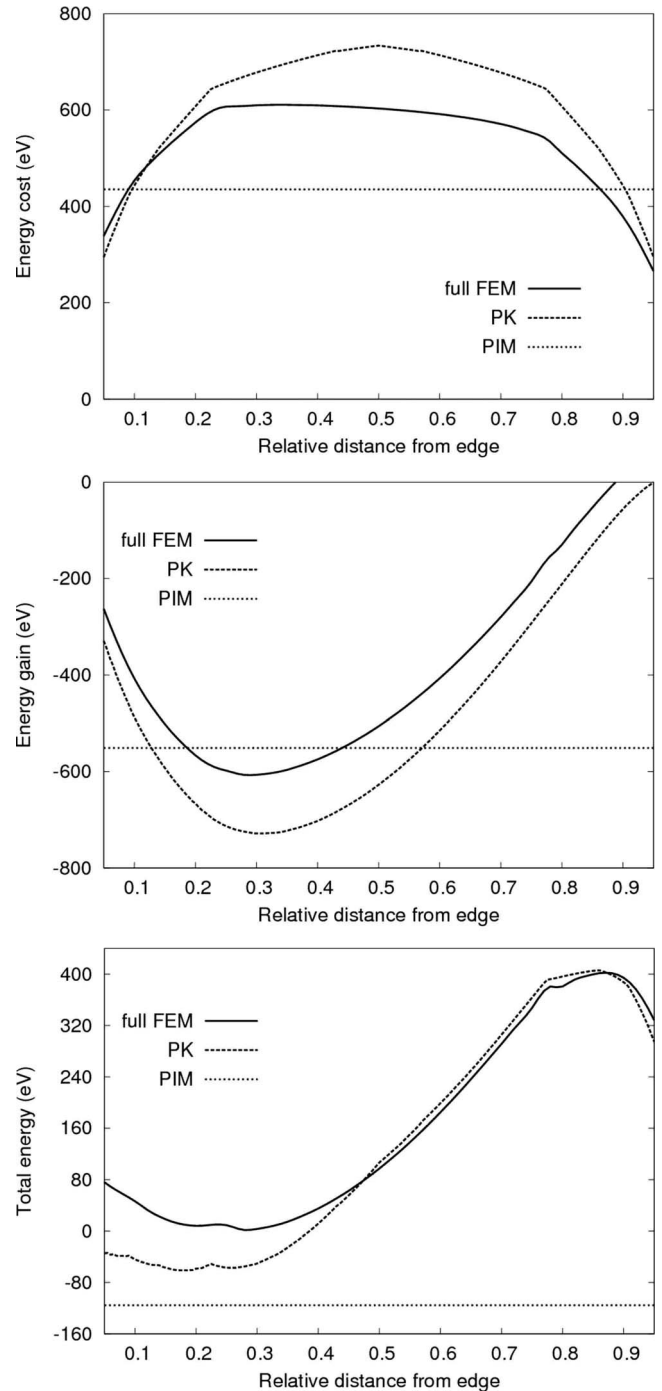
FIG. 8. Comparison between full FEM, PK, and PIM results for a barn island with base $L = 35$ nm. The first panel reports the values of E_{cost}, the middle panel those of E_{gain}, and the bottom panel those of E_{tot}.

is that the PK curve is symmetric, merely reflecting the barn geometry, while the full FEM curve correctly shows a behavior determined by the dependence of the elastic field on the relative orientation of the different surfaces and the Burgers vector. Since at the two opposite island edges the facet normal is differently oriented, a different E_{cost} must be expected. The effect of the relative-orientation-dependent elastic field revealed by full FEM is particularly important in nanometric
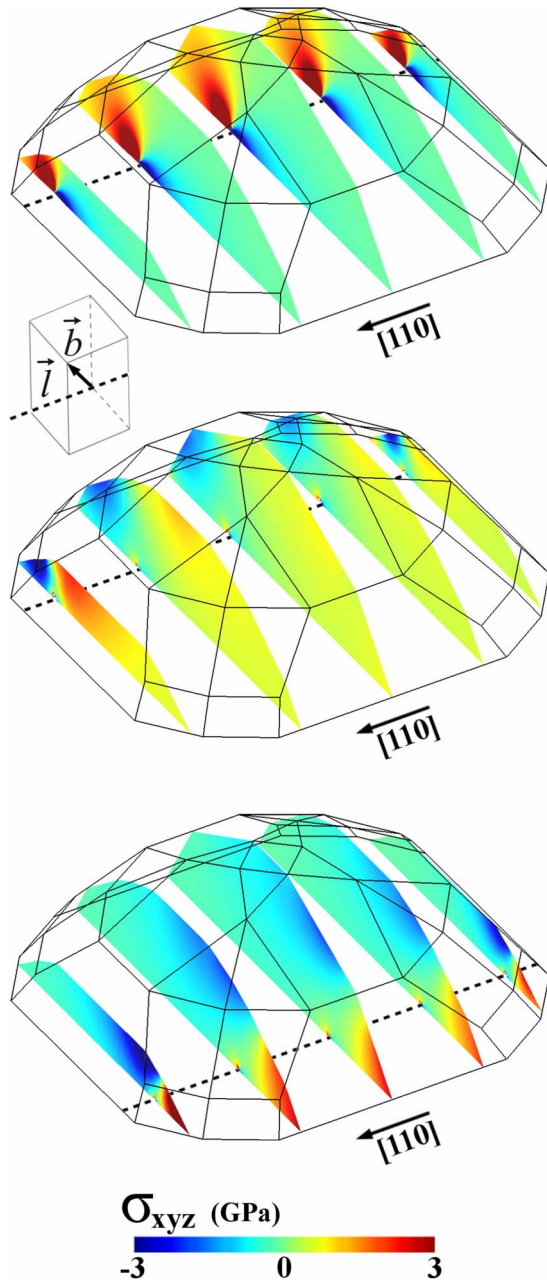
FIG. 9. (Color online) Color maps of the hydrostatic stress in different cross sections of the barn cut along the dislocation line ($\vec{l}$). Shown in the upper panel is the analytical dislocation segment bulk solution $\sigma_{xyz}^{dislo}(\mathbf{u})$ (cut following the barn shape). The defect is located in the position corresponding to the E_{tot} minimum. The central and the lower panels describe only the dislocation-surface interaction $[\sigma_{xyz}^{surf}(\mathbf{u}) + \sigma_{xyz}^{int}(\mathbf{u})]$: the former refers to the same position of the upper panel, and the latter to a symmetric position on the other island side.

multifaceted island, where the dislocation line turns to be always close to a free surfaces; it is investigated here in detail.

In Fig. 9 the role played by the free surfaces (and the interface) is made clear by plotting the difference between the hydrostatic stresses for the equilibrium solution when only the dislocation segment is present and the dislocation

analytical bulk solution (reported in the upper panel).[21] That is, following the definitions in Sec. II, Fig. 9 shows $\sigma_{xyz}^{tot}(\mathbf{u}) - \sigma_{xyz}^{dislo}(\mathbf{u}) = \sigma_{xyz}^{surf}(\mathbf{u}) + \sigma_{xyz}^{int}(\mathbf{u})$. The middle panel displays the behavior obtained by placing the dislocation at the position corresponding to the minimum of the E_{tot} curve and the lower one reports the data obtained when the dislocation is in a symmetric position on the other island side. Notice that the $\sigma_{xyz}^{surf}(\mathbf{u}) + \sigma_{xyz}^{int}(\mathbf{u})$ actually reduces the dislocation field (upper panel), being opposite in sign. Indeed the E_{cost} found in the PK approach results higher with respect to the full FEM one because of the too simple approximation used for the surface contribution that corresponds to a simple geometric cutoff of the dislocation field. The comparison between the middle and the bottom panels highlights the dislocation-position dependence of the surface terms that gives rise to the asymmetry in the full FEM E_{cost} curve. From Fig. 9 we conclude also that no significant effect seems to be present due to the Ge/Si interface at the bottom of the island $[\sigma_{xyz}^{int}(\mathbf{u})$; see Sec. II] mainly because of the very similar values of the elastic constants of the two materials.

Let us now focus our attention on the E_{gain} term, reported in the central panel of Fig. 8. Actually, the Peach-Koehler force is shown to yield a good qualitative description of the interaction between the dislocation field and the epitaxial one. Indeed, the use of the FEM-computed elastic field in the island before the onset of the plastic relaxation in the PK expressions guarantees a correct estimation of the energy reduction obtained when a dislocation is introduced. Very importantly, the PK and full FEM curves present the minimum at the same position along the interface (~ 0.3), so the two models predict the same equilibrium dislocation position. It is important to notice that such position, maximum in the energy reduction, actually corresponds to a strong release of the island edge compression due to the expansive lobe of the dislocation field (see upper right panel of Fig. 2). From the quantitative point of view, the energy gain seems to be overestimated instead by the PK approach. Since the same behavior was found for E_{cost} (opposite in sign), the total-energy curve is expected to benefit from this compensation. Indeed, by looking at the bottom panel of Fig. 8, one sees that full FEM and PK give very close results in the central region. It is evident, instead, the failure of the PK-based approach when the dislocation is in the proximity of the island edge closer to E_{tot} minimum position. Notice that such minimum for the full FEM calculation corresponds to 0 eV. This is because the comparison reported in this section was performed exactly at the full FEM critical volume for dislocation introduction. Section V is dedicated to a more detailed investigation of critical volumes, including a comparison to Ge concentration-dependent experimental data.

Up to now we have focused our attention on the comparison between the full FEM and PK results since they allowed for a detailed analysis of position-dependent energy contributions. Still the three panels of Fig. 8 also report the result predicted by the simplest PIM approach. It is evident that the E_{cost} term value is strongly underestimated when compared with the corresponding values obtained by the two other methods at the position which maximizes strain relaxation. Evidently, the strongly simplified description of the effective cutoff used by PIM is not sufficient to reproduce the real

effect of free surfaces on the dislocation field in the island. Moreover, the expression of E_{gain}, described as the simple misfit reduction in the island, turns out to be an underestimation of the real energy gain. Mainly, as revealed, for instance, by looking at Fig. 3, the dislocation field plays an important role also in the reduction in the substrate expansion below the island, due to the elastic relaxation. This contribution to the energy gain is completely absent in the PIM approach [while it is taken into account in the PK one by the use of the FEM calculated $\hat{\sigma}(x,y,z)$ in the E_{gain} expression]. However, a compensation effect similar to the one observed for the PK approach is taking place, but in this case the deviation of E_{tot} from the full FEM value is still relevant.

V. PREDICTION OF THE CRITICAL SIZE VERSUS EXPERIMENTS

A useful and interesting application of the methods described above is the calculation of the critical island dimension for the onset of plastic relaxation. Such calculation has already been published in the Peach-Koehler framework for SiGe islands[19] and in a PIM approach for the GaAs one.[42] Here we compare the PK results with the one obtained using the more accurate full FEM approach and the simplest PIM one. Critical volumes V_C are defined as the smaller island dimensions where there exists at least one dislocation position where $E_{gain}=-E_{cost}$. Clearly, finding V_C requires calculating the two terms for different island sizes and, except for the PIM approach, for different dislocation positions along the interface. If in Secs. II–IV we simply considered pure Ge islands, here we wish to carry out the calculations at realistic Ge compositions. We considered values ranging between 20% and 70% as determined in Ref. 19 by using different growth temperatures. In the FEM calculations, alloying can be tackled by considering a rescaled misfit stress (and a correspondingly smaller f in the PIM approach), $\sigma_m=-8.6x_{Ge}$ GPa, where x_{Ge} is the Ge content, and also linearly interpolated elastic constants $[C_{ij}^{SiGe}(x_{Ge})=x_{Ge}C_{ij}^{Ge}+(1-x_{Ge})C_{ij}^{Si}]$. Results, obtained by full FEM, PK, and PIM are displayed in Fig. 10, along with the experimental data of Ref. 19. With respect to that work, here only the data where the concentration values were determined by independent and more accurate x-ray measurements are shown. In the plot, the vertical axis represent the barn critical island base, experimentally estimated by looking at the internal plateau regions revealed by selective etching.[19] Let us first focus on the three models.

While the three theoretical curves all capture the essential physics (higher Ge concentrations determine larger elastic-energy accumulation, and, therefore, smaller critical volumes), a closer comparison reveals once again the different levels of approximation, with full FEM yielding a virtually exact description. The sizable underestimation of the E_{cost} term in the PIM approach, as expected, yields too small critical sizes, a similar behavior being displayed also by the PK method, where we have noticed some overestimation in the energy gain. Interestingly, despite the approximations discussed in Sec. IV, critical island dimensions predicted by the PK method, as well as by the extremely simple PIM, do not
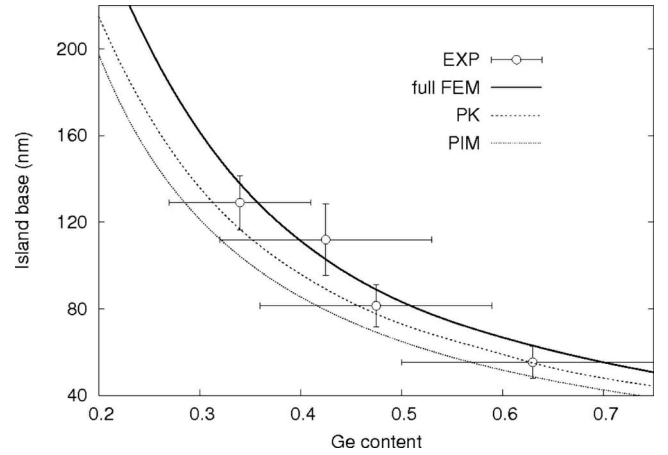
FIG. 10. Critical island bases as calculated by the three presented methods and compared with the experimental data of Ref. 19.

deviate substantially from the full FEM results, particularly if one takes into account the large experimental uncertainties on the actual Ge content. However, it is well visible that the most accurate full FEM approach better recovers the data. Overall, the agreement between the latter and experiments is very satisfactory and reinforces the main conclusion of Ref. 19: dislocation injection in nanometric island is not kinetically limited all along the concentration (and, thus, the temperature) range, at variance to the flat film case.

As a final investigation, we carried out a comparison between the thermodynamic critical heights in islands and in flat films. Using only the FEM approach, the critical heights h_c determining dislocation injection in films have been determined for the same concentration values previously considered for the barns, together with the pure Ge case. It may appear of limited interest to investigate the very Ge-rich case, where flat films can be grown only by freezing the surface atomistic diffusion [i.e., using a high H concentration in plasma-enhanced chemical-vapor deposition (PECVD) growth]. Still, in this case h_c is very small, and the role of the
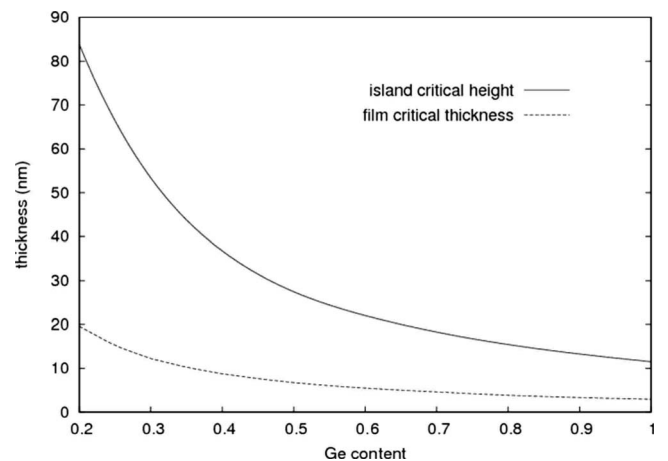
FIG. 11. Critical thickness for flat films (dashed line), as compared to the barn island height (solid line), both calculated by full FEM.

surfaces is much larger and the one of threading arms is much smaller. In Fig. 11, h_c is compared with the corresponding height of barn islands at the critical volume. It is evident that from the thermodynamic point of view, higher structures can be reached before the onset of plastic relaxation in a three-dimensional growth with respect to the two-dimensional one, the effect being particularly pronounced at low misfit values. The result is easily understood in the simpler PIM picture: the function $F_\nu(\rho)$ is equal to 1 for flat film, giving rise to a larger energy gain with respect to islands where $F_\nu(\rho) < 1$, so that the latter critical dimensions have to be higher. However, at variance with islands, measured values for critical films seem much higher than the thermodynamic predictions,[32,45] highlighting a key role of the kinetic barriers opposing the dislocation nucleation in films.

VI. CONCLUSIONS

In this work a detailed investigation of the effects of plasticity at the onset of dislocation injection in heteroepitaxial SiGe islands on Si has been presented. A virtually exact FEM treatment has been used to investigate several dislocation-position-dependent features of the stress field, and to estimate critical volumes for realistic 3D islands. Two other approaches, based on different levels of approximations, were also applied to the same problem. Their comparison provides valuable insights into the role played by dislocation-surface interaction in a multifaceted object, correctly described by FEM. Theoretical results were compared with available experimental data, finding very satisfactory agreement and demonstrating the predicting power of a thermodynamic approach to plasticity onset, at variance with the two-dimensional thin-film case.

*Corresponding author; riccardo.gatti@mater.unimib.it

[1] V. A. Shchukin and D. Bimberg, Rev. Mod. Phys. **71**, 1125 (1999).

[2] Y. W. Mo, D. E. Savage, B. S. Swartzentruber, and M. G. Lagally, Phys. Rev. Lett. **65**, 1020 (1990).

[3] D. J. Eaglesham and M. Cerullo, Phys. Rev. Lett. **64**, 1943 (1990).

[4] V. A. Zinovyev, G. Vastola, F. Montalenti, and L. Miglio, Surf. Sci. **600**, 4777 (2006).

[5] J. Stangl, V. Holy, and G. Bauer, Rev. Mod. Phys. **76**, 725 (2004).

[6] G. Costantini, A. Rastelli, C. Manzano, R. Songmuang, O. G. Schmidt, K. Kern, and H. von Kanel, Appl. Phys. Lett. **85**, 5673 (2004).

[7] F. Ratto, G. Costantini, A. Rastelli, O. G. Schmidt, K. Kernz, and F. Rosei, J. Exp. Nanosci. **1**, 279 (2006).

[8] G. Medeiros-Ribeiro, A. M. Bratkovski, T. I. Kamins, D. A. A. Ohlberg, and R. S. Williams, Science **279**, 353 (1998).

[9] E. Sutter, P. Sutter, and J. E. Bernard, Appl. Phys. Lett. **84**, 2262 (2004).

[10] M. Stoffel, A. Rastelli, J. Tersoff, T. Merdzhanova, and O. G. Schmidt, Phys. Rev. B **74**, 155326 (2006).

[11] G. Vastola, R. Gatti, A. Marzegalli, F. Montalenti, and Leo Miglio, in *Self-Assembled Quantum Dots*, edited by Zhiming M. Wang (Springer, Berlin, 2008), pp. 421–438.

[12] F. K. LeGoues, M. C. Reuter, J. Tersoff, M. Hammar, and R. M. Tromp, Phys. Rev. Lett. **73**, 300 (1994).

[13] F. M. Ross, J. Tersoff, M. C. Reuter, F. K. LeGoues, and R. M. Tromp, Microsc. Res. Tech. **42**, 281 (1998).

[14] A. Rastelli, M. Kummer, and H. von Kanel, Phys. Rev. Lett. **87**, 256101 (2001).

[15] G. Capellini, M. De Seta, and F. Evangelisti, Appl. Phys. Lett. **78**, 303 (2001).

[16] M. Floyd, Y. Zhanga, K. P. Driver, J. Drucker, P. A. Crozier, and D. J. Smith, Appl. Phys. Lett. **82**, 1473 (2003).

[17] T. U. Schülli, M. Stoffel, A. Hesse, J. Stangl, R. T. Lechner, E. Wintersberger, M. Sztucki, T. H. Metzger, O. G. Schmidt, and G. Bauer, Phys. Rev. B **71**, 035326 (2005).

[18] T. Merdzhanova, S. Kiravittaya, A. Rastelli, M. Stoffel, U. Denker, and O. G. Schmidt, Phys. Rev. Lett. **96**, 226103 (2006).

[19] A. Marzegalli, V. A. Zinovyev, F. Montalenti, A. Rastelli, M. Stoffel, T. Merdzhanova, O. G. Schmidt, and Leo Miglio, Phys. Rev. Lett. **99**, 235505 (2007).

[20] Z. Y. Zhong, W. Schwinger, F. Schaffler, G. Bauer, G. Vastola, F. Montalenti, and Leo Miglio, Phys. Rev. Lett. **98**, 176102 (2007).

[21] J. P. Hirth and J. Lothe, *Theory of Dislocations* (Krieger, Malabar, 1992).

[22] M. Peach and J. S. Koehler, Phys. Rev. **80**, 436 (1950).

[23] B. J. Spencer and J. Tersoff, Phys. Rev. B **63**, 205424 (2001).

[24] J. F. Justo, A. Fazzio, and A. Antonelli, J. Phys.: Condens. Matter **12**, 10039 (2000).

[25] A. T. Blumenau, M. I. Heggie, C. J. Fall, R. Jones, and T. Frauenheim, Phys. Rev. B **65**, 205205 (2002).

[26] I. N. Remediakis, D. E. Jesson, and P. C. Kelires, Phys. Rev. Lett. **97**, 255502 (2006).

[27] E. Van der Giessen and A. Needleman, Modell. Simul. Mater. Sci. Eng. **3**, 689 (1995).

[28] R. Gracie, J. Oswald, and T. Belytschko, J. Mech. Phys. Solids **56**, 200 (2008).

[29] B. Devincre, L. P. Kubin, C. Lemarchand, and R. Madec, Mater. Sci. Eng., A **309-310**, 211 (2001).

[30] T. Belytschko and R. Gracie, Int. J. Plast. **23**, 1721 (2007).

[31] J. W. Matthews and A. E. Blakeslee, J. Cryst. Growth **27**, 118 (1974).

[32] R. Hull in *Properties of Silicon Germanium and SiGe: Carbon*, edited by Erich Kasper and Klara Lyutovich (University of Stuttgart, Germany, 2000), pp. 21–39.

[33] A. K. Head, Proc. Phys. Soc. London, Sect. B **66**, 793 (1953).

[34] H. T. Johnson and L. B. Freund, J. Appl. Phys. **81**, 6081 (1997).

[35] R. Gracie, G. Ventura, and T. Belytschko, Int. J. Numer. Methods Eng. **69**, 423 (2007).

[36] J. Zou, X. Z. Liao, D. J. H. Cockayne, and Z. M. Jiang, Appl. Phys. Lett. **81**, 1996 (2002).

[37] J. Tersoff, Phys. Rev. B **37**, 6991 (1988).

[38] J. Tersoff, Phys. Rev. B **39**, 5566 (1989).

[39] A. Marzegalli, F. Montalenti, and Leo Miglio, Appl. Phys. Lett. **86**, 041912 (2005).

[40] A. Marzegalli, F. Montalenti, and Leo Miglio, J. Phys.: Condens. Matter **17**, 7505 (2005).

[41] While introducing a 3 ML WL does not require any additional cost in the atomistic simulations, so that we considered its presence, inserting a three-layer Ge subdomain in the FEM calculation forces the creation of a dense mesh within this thin region. Since the WL has a negligible effect on the island stress field (Ref. 9) (as also demonstrated by the comparison between atomistic and FEM results), we avoided this additional computational cost in the FEM calculations by placing the island directly on the Si substrate. We also checked that neglecting the WL does not produce any significant variation in the critical volume for dislocation insertion.

[42] K. Tillmann and A. Förster, Thin Solid Films **368**, 93 (2000).

[43] F. Glas, Phys. Rev. B **74**, 121302(R) (2006).

[44] As discussed when describing the PK and the MF approaches, the presence of free surfaces causes a faster decay of the dislocation field. This allowed us to find converged values of E_{tot} considering relatively thin substrates. For the results reported in Sec. IV, a Si substrate thickness of 2000 nm turned out to be more than sufficient.

[45] D. C. Houghton, J. Appl. Phys. **70**, 2136 (1991).